Solar Energy Materials & Solar Cells 140 (2015) 38–44

Contents lists available at ScienceDirect

Solar Energy Materials & Solar Cells

journal homepage: www.elsevier.com/locate/solmat

Passivated contacts to laser doped p^+ and n^+ regions

Xinbo Yang*, James Bullock, Lujia Xu, Qunyu Bi, Sachin Surve, Marco Ernst, Klaus Weber

Research School of Engineering, The Australian National University, Canberra, ACT 2601, Australia

ARTICLE INFO

Article history:
Received 13 November 2014
Received in revised form
20 March 2015
Accepted 23 March 2015
Available online 14 April 2015

Keywords:
Passivated contact
Laser doping
Tunnel oxide
Interdigitated back-contact cell

ABSTRACT

In this work, tunnel SiO_2/a-Si:H stacks are trialed as passivated contacts to laser doped p^+ and n^+ regions. The passivation performance and contact resistivity are investigated as a function of the tunnel SiO_2 thickness and annealing condition. We find that the SiO_2/a-Si:H stack provides excellent passivation to laser doped n^+ regions, with corresponding low recombination current density (J_o) values. A lower level of surface passivation is achieved by the SiO_2/a-Si:H stack on laser doped p^+ regions. A post-deposition forming gas anneal (FGA) at 400 °C is found to improve the passivation performance to laser doped p^+ regions and deteriorate the passivation to laser doped n^+ regions. Acceptable contact resistivity (ρ_c) values have been obtained for both laser doped n^+ and p^+ regions after aluminum metallization and a post FGA to activate the alloying process between the a-Si:H and aluminum layer. In the final part of this work implementation of the passivated contacts to laser doped regions into a simplified interdigitated back-contact (IBC) solar cell fabrication process is proposed. Simulation result suggests that IBC device with an efficiency of up to 23% can be achieved using the obtained experimental results.

1. Introduction

The main challenge in today's solar cells industry is to increase the conversion efficiency and to lower the production costs of cells. State-of-the-art high efficiency silicon solar cells, such as the passivated-emitter rear locally diffused (PERL) cell [1] and interdigitated back-contact (IBC) cell [2], are fabricated with locally doped regions at front and/or rear sides of the cell. However, the approach to realize local doping requires cost-intensive and time-consuming processes such as photolithography and high temperature diffusions, the cost of which prevents the integration of these cell concepts into mass production.

In recent years, laser processing has attracted considerable attention as a fast and cost-effective technique for forming locally doped regions in silicon solar cells. High efficiency silicon solar cells with laser-doped selective emitter (SE) or/and local back surface field (LBSF) have been reported [3–10], and an absolute efficiency gain up to 1% could be achieved. Laser processed IBC solar cells with efficiencies up to 22% have also been successfully fabricated without the necessity of any masking, and the fabrication process has been significantly simplified [11]. Nevertheless, the laser-doped region usually exhibits a high carrier recombination because of the laser-induced defects [12,13]. Recent simulation results have indicated that the recombination current density of laser doped regions without passivation may be higher than 5000 fA/cm^2 (even reaching a few tens of thousand fA/cm^2 with non-optimized laser parameters), which is much higher than that of diffused regions [14]. Therefore, the high recombination at the laser doped regions has limited the performance of the laser-processed solar cells.

Generally, the fraction of laser doped regions are optimized and reduced to a certain low limit to minimize the recombination loss, which in turn improves the open circuit voltage (V_{oc}) of the solar cell. However, further decreases in the area of laser doped regions could increase the contact resistance, and therefore decrease the fill factor (FF). The trade-off between V_{oc} and FF has to be considered when decreasing the fraction of laser doped regions. An alternative approach is to passivate the laser doped regions with an ultra-thin dielectric, which have to be sufficiently thin to allow current flow whilst being thick enough to provide reasonable surface passivation. Silicon solar cells featuring an ultra-thin dielectric layer under the contact, referred to as a metal–insulator–semiconductor (MIS) contact, have been developed since the 1980 s. A thermally grown ultra-thin SiO_2 layer was firstly implemented under the front contact by Green et al. in their metal–insulator n^+p (MINP) type solar cells [15]. Similarly, an efficiency of up to 21.1% has been achieved by MIS-contacted silicon solar cells featuring a tunnel SiO_2 under the front aluminum contact [16,17]. Recently, ultra-thin Al_2O_3 and amorphous silicon (a-Si:H) films have also been investigated as the MIS contacts for silicon solar cells [18–21]. The results indicated that Al_2O_3 and a-Si:H

* Corresponding author. Tel.: +61 2 6197 0112; fax: +61 2 6125 0506.
E-mail address: xinbo.yang@anu.edu.au (X. Yang).

http://dx.doi.org/10.1016/j.solmat.2015.03.026
0927-0248/

ultrathin layers with optimized thickness could provide appreciable passivation to diffused p^+ and n^+ regions whilst maintaining a relatively low contact resistivity. However, the passivation stability of these ultrathin dielectrics during the final metal contact annealing is still a problem to be resolved before being applied to solar cell.

Recently, the SiO_2/a-Si:H and Al_2O_3/a-Si:H stacks, have been developed as enhanced MIS passivated contacts to diffused n^+ and p^+ regions, respectively [22,23]. The stacks show excellent passivation to diffused n^+ and p^+ regions as well as high thermal stability up to 350 °C. The contact formation is achieved by aluminum metallization and annealing to activate the alloying process between the a-Si:H and aluminum layer, which has previously been investigated for low-temperature p–n junction formation [24,25]. A low-cost, low-temperature processing of rear-passivated locally contacted Si solar cells has also been proposed by applying the contacts to a-Si:H passivated wafers by means of the annealing (COSIMA) method [26]. Recently, high efficiency n-type silicon solar cells featuring a SiO_2/a-Si:H passivated contact to diffused or laser doped n^+ regions at the rear have been developed [27,28]. In this work, the SiO_2/a-Si:H stack is applied as the passivated contacts to both laser doped n^+ and p^+ regions, and the passivation quality, contact resistivity and thermal stability are investigated by the quasi-steady-state photoconductance (QSSPC) technique [29], the transfer length method (TLM) [30] and photoluminescence (PL) imaging [31]. The final section of this paper proposes that simplified IBC solar cells could be fabricated with the proposed passivated contact on localized laser doped n^+ and p^+ regions. Simulations demonstrate that an efficiency of up to 23.0% is possible with non-optimized parameters.

2. Experimental

Laser doping was carried out on (100)-oriented FZ silicon wafers with high base resistivity ($>100\ \Omega$ cm). For samples with laser doped n^+ regions, surface damage etched p-type substrates with a thickness of ~450 μm were used and vice versa for laser doped p^+ regions. Phosphorus or boron spin-on-dopant solutions (P-SOD/B-SOD, Filmtronics Inc.) were used as dopant sources. After RCA cleaning, P-SOD or B-SOD was spun on the front surface, followed by baking in an oven at 90 °C in air ambient. A KrF excimer laser (248 nm) with the pulse duration of 20 ns was used for laser doping. A $70\times70\ mm^2$ area was laser doped with selected laser fluences on 4 in. wafers. After HF dip and RCA cleaning, the rear side was spun on with the same dopant solution and then laser doped with the same fluence to form the symmetrical test structure for QSSPC measurement. The sheet resistance (R_{sheet}) variation was controlled within 5%. Next the double-side laser-doped wafers were quartered, and the R_{sheet} of the laser doped p^+ and n^+ regions was measured by a four point probe. Then the electrically active dopant profile was measured by the electrochemical capacitance-voltage (ECV) profiling technique [32].

Following another RCA clean, the laser doped samples were subjected to a short thermal oxidation in a clean quartz tube furnace at 800 °C for different times (typically < 60 s), resulting in SiO_2 thickness between 1.3 and 2.0 nm. The SiO_2 film thicknesses were determined by ellipsometry by fitting polarized reflectance data of single side polished wafers, which had a phosphorus or boron diffusion with a similar surface concentration. Then an a-Si:H (~30 nm) film was deposited on both sides of the samples by PECVD. Selected samples were forming gas annealed (FGA) at different temperatures, and the recombination current density (J_o) of the samples was obtained by the QSSPC technique using the high injection method [33] with an intrinsic carrier concentration $n_i=8.6\times10^9\ cm^{-3}$ (at 297 K). Aluminum (~1 μm) was then evaporated on one side of the samples with SiO_2/a-Si:H passivation stack, and a transfer length method (TLM) pattern was defined using photolithography. Pad spacings of 10–300 μm were used here. After cleaving into $20\times6\ mm^2$ TLM strips, these samples were annealed in FGA at different temperatures for different times. Current–voltage measurements were performed on a Keithley 2425 Source Meter. The contact resistivity (ρ_c) was obtained from an extrapolation of resistance versus pad spacing. The passivation stability after FGA at different temperatures was monitored by PL image with a short pass filter (1025 nm), which minimizes the effect of rear-side reflection.

Using the measured J_o and ρ_c parameters of laser doped p^+ and n^+ regions with SiO_2/a-Si:H passivation stacks, an IBC solar cell with localized laser doped p^+ and n^+ regions was simulated using the IBC version of Quokka, capable of simulating a 2-D/3-D unit cell with a variety of interdigitated contact and doping patterns [34]. The free energy loss analysis has been implemented in Quokka, providing a full quantitative loss analysis of both resistive and recombinative losses.

3. Results and discussion

3.1. Passivation performance of the SiO_2/a-Si:H stacks on laser doped n^+ and p^+ regions

Table 1 shows the basic properties of the laser doped n^+ and p^+ regions used in this study. Compared with similar R_{sheet} diffused n^+ and p^+ regions, the laser doped regions show a relatively higher surface concentration (N_{surf}) and shallower junction depth. Fig. 1 shows the typical ECV profiles of laser doped n^+ and p^+ regions (sample n^+-1 and p^+-1), which exhibit a N_{surf} of 2.8×10^{19} and $1.9\times10^{19}\ cm^{-3}$ at a relatively high R_{sheet} of 280 and 490 Ω/□, respectively. The high N_{surf} of laser doped regions could be beneficial for the contacting. The un-passivated J_o values ($J_{o,un\text{-}pass}$) were extracted from an imperfect linear fitting using the Kane and Swanson technique [33], and these high values may still be under estimations according to previous simulations [14]. The passivated J_o values ($J_{o,pass}$) were obtained via PECVD SiN_x (~70 nm) for laser

Table 1
Electrical properties of laser doped n^+ and p^+ regions.

Samples	R_{sheet} (Ω/□)	N_{surf} (cm^{-3})	$J_{o,un\text{-}pass}$ (fA/cm^2)	$J_{o,pass}$ (fA/cm^2)
n^+-1	280 ± 10	2.8×10^{19}	1850 ± 200	50 ± 5
n^+-2	190 ± 10	3.3×10^{19}	1590 ± 100	90 ± 5
p^+-1	490 ± 10	1.9×10^{19}	3100 ± 300	100 ± 20
p^+-2	196 ± 10	4.0×10^{19}	2200 ± 200	260 ± 20

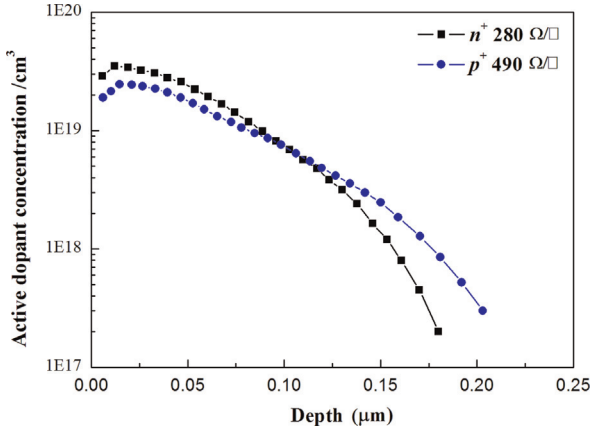

Fig. 1. Typical ECV profiles of the laser doped n^+ and p^+ regions.

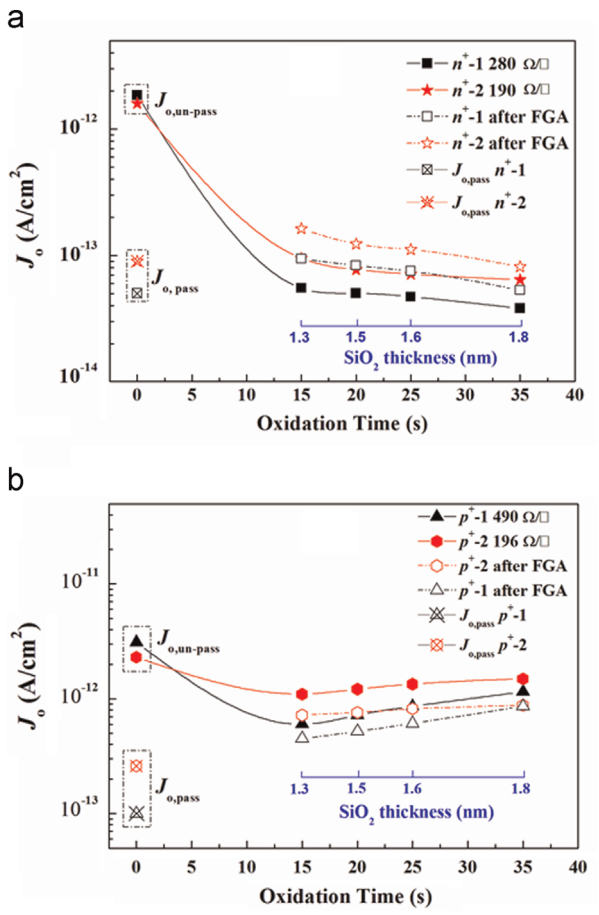

Fig. 2. The J_o values of laser doped (a) n^+ and (b) p^+ regions passivated by SiO_2/a-Si:H stack as a function of oxidation time at 800 °C. The approximate SiO_2 thickness is shown on the floating axis. The J_o values after FGA at 400 °C for 30 min as well as the $J_{o,un\text{-}pass}$ and $J_{o,\ pass}$ are also shown. Lines only provide a guide to the eyes.

doped n^+ regions and ALD Al_2O_3 (~20 nm) for laser doped p^+ regions, respectively. These J_o values are muc`h higher than those obtained for diffused n^+ and p^+ emitters with the same passivation layers [35,36], which could be attributed to the laser-induced defects as well as the relatively high N_{surf}.

Fig. 2 shows the J_o value dependence on oxidation time for laser doped n^+ and p^+ regions passivated by the SiO_2/a-Si:H stack. The J_o values of these samples after FGA annealing at 400 °C for 30 min as well as the $J_{o,un\text{-}pass}$ and $J_{o,pass}$ values listed in Table 1 are shown together. The approximate SiO_2 thickness with different oxidation times is also included. The SiO_2/a-Si:H stack can provide excellent passivation to laser doped n^+ region, and the obtained J_o values are close to or even lower than those obtained with SiN_x passivation. As the oxidation time increases, the J_o values decrease for n^+ regions with different R_{sheet}. An oxidation of 35 s at 800 °C (SiO_2 thickness ~1.8 nm) could achieve a low J_o value of 38 and 64 fA/cm^2 on the laser doped n^+ regions with a R_{sheet} of 280 and 190 Ω/□, respectively. However, the passivation performance of SiO_2/a-Si:H stack on laser doped n^+ regions degraded after FGA at 400 °C for 30 min. The J_o values increase on average by ~60%, which may be attributed to the de-hydrogenation during the FGA annealing. Whereas the passivation performance of the SiO_2/a-Si:H stack on laser doped p^+ regions is lower, as shown in Fig. 2b. The minimum J_o values of 600 and 1100 fA/cm^2 are achieved for laser doped p^+ regions with the R_{sheet} of 490 and 196 Ω/□, respectively. These J_o values are much higher than $J_{o,\ pass}$ values (100 and 260 fA/cm^2) obtained with the Al_2O_3 passivation. Surprisingly the J_o value is seen to increase as the oxidation time (SiO_2 thickness) increases and a post FGA anneal at 400 °C for 30 min could improve the passivation quality to some extent. Both results are opposite to those obtained on laser doped n^+ regions.

The reason for the different passivation behavior of the SiO_2/a-Si:H stack on laser doped p^+ and n^+ regions is not fully understood at the point. One possible explanation is that different passivation mechanisms have to be applied to the laser doped p^+ and n^+ regions with the same SiO_2/a-Si:H passivation stack. The n^+ region mainly relies on the passivation of tunnel SiO_2 and the p^+ region mainly relies on the passivation of a-Si:H. The a-Si:H film has shown a good surface passivation to diffused p^+ regions [21]. With increasing oxidation time and therefore SiO_2 thickness, the passivation quality to n^+ regions could be improved. However, the increasing SiO_2 thickness may block the hydrogen diffusion from the a-Si:H to the SiO_2/Si interface, which deteriorates the passivation quality of a-Si:H to p^+ regions. A post-deposition FGA anneal at 400 °C may cause de-hydrogenation of the Si–SiO_2 interface for the n^+ regions and help the hydrogen diffusion from the a-Si:H to the SiO_2/Si interface for the p^+ regions, which may lead to the passivation degradation to n^+ regions and improvement to p^+ regions. Nevertheless, it is still an open question for further investigation.

3.2. Contact resistivity as a function of FGA conditions

Although the SiO_2/a-Si:H stack could provide appreciable passivation to laser doped p^+ and n^+ regions, the contact resistivity has to be investigated before being applied to solar cells. The contact formation will occur during annealing at certain temperature at which the a-Si:H and aluminum alloying interaction will happen. Fig. 3 shows the contact resistivity (ρ_c) dependence of FGA anneal condition for laser doped n^+ and p^+ regions with different oxidation times. The directly metalized ρ_c values are shown as a reference. Laser doped n^+ and p^+ regions with oxidation time of 35 s exhibit non-ohmic contact for all FGA conditions, which is not shown in Fig. 3. A typical solar cell final contact annealing, FGA at 250 °C for 30 min, could achieve an acceptable ρ_c values for both n^+ (9.6×10^{-4} Ω cm^2) and p^+ (5.7×10^{-3} Ω cm^2) contacts. An obvious increase in ρ_c is observed with the increasing oxidation time (SiO_2 thickness) under the same FGA condition. As the FGA anneal temperature and time increase, the ρ_c value decreases continuously. The current transport across the interfacial oxide is considered to be mainly dominated by tunneling through the oxide [37] when annealed at a relatively low temperature. However, current transport through oxide pinholes, which might form during a high temperature annealing, may also act as an additional transport mechanism. The current transport through oxide pinholes instead of tunneling has been widely investigated and accepted in the SiO_2/poly-Si passivated contacts after annealing at a high temperature [38–40]. The sharp decrease of ρ_c values after annealing at a high temperature might be partly attributed to the additional current transport through oxide pinholes.

With the decreasing ρ_c values after FGA anneal, it is important to maintain the passivation performance simultaneously. It has previously been suggested that the PL intensity is inversely proportional to J_o at any injection level [41], and here PL images taken with a short pass filter was used to qualitatively monitor the changes in passivation after each FGA anneal step. The PL images of these TLM strips show different PL intensities (I_{PL}) after different FGA steps, as shown in Fig. 4, which indicates that the passivation changes. All the PL images of laser doped n^+ regions were acquired with the same PL parameters, and so were the p^+ regions. However, the n^+ and p^+ regions were acquired with different PL parameters, and hence they cannot be compared directly. Actually, the I_{PL} of laser doped n^+ region is much higher than that of p^+ regions when acquired with the same PL parameters, which reflects the large difference in J_o

values with the SiO_2/a-Si:H passivation stack. The I_{PL} changes of the samples during the FGA processes are most likely attributable to the interaction between the a-Si:H and aluminum at the rear. We have investigated the effect of FGA anneal at 250 °C or 300 °C and only a slight difference in the passivation quality of laser doped n^+ and p^+ regions was found. Therefore, the I_{PL} changes at the front side of the samples during the FGA can be neglected.

After Al metallization, the I_{PL} of laser doped n^+ regions increase as the oxidation time increases (Fig. 4a), which is consistent with the decreasing J_o values shown in Fig.2a. After FGA at 250 °C for 30 min, the I_{PL} of all the samples decreases, which indicates that the passivation quality degrades during the FGA. Samples which experienced shorter oxidation times show larger I_{PL} decrease and therefore stronger degradation (e.g. the first TLM strip). Fortunately, the I_{PL} of the sample with the oxidation time of 25 s decreases only slightly (~8%), which indicates that the passivation quality is mostly maintained during the FGA anneal at 250 °C. An acceptable ρ_c value of $9.6 \times 10^{-4}\ \Omega\ cm^2$ has been achieved on this sample, which indicates that alloying between the a-Si:H and Al has occurred and hence contact formation has been achieved during the FGA at 250 °C. With increasing FGA temperature and time, an obvious I_{PL} decrease and therefore passivation quality degradation was observed for the first three samples. Although the sample with the oxidation time of 35 s only shows slight I_{PL} changes during all the FGA anneal processes, non-ohmic behavior is obtained on this sample. The PL images show that the passivated contact to laser doped n^+ regions is stable at 250 °C for the sample with the oxidation time of 25 s. Bullock et al. reported that the same passivated contact to diffused n^+ regions could be stable up to 350 °C [23]. The difference may be attributed to the rough surface of laser doped n^+ regions which causes non-uniform tunnel SiO_2 growth during the oxidation, which is supported by the the non-uniform I_{PL} of the TLM strips after Al metallization. As the annealing temperature increases, the Al accumulated at the ultra-thin SiO_2 surface during the alloying process may react with SiO_2, and therefore cause the degradation of surface passivation.

The PL images of laser doped p^+ regions exhibit a different I_{PL} change after FGA annealing, which reflects the different J_o value changes shown in Fig.2b. After FGA anneals at 250 °C for 30 min, the I_{PL} decreases slightly for all the samples due to the alloying at the rear side. An increasing ρ_c value of 5.8×10^{-4}, 2.7×10^{-3} and $5.7 \times 10^{-3}\ \Omega\ cm^2$ is observed at this stage for the samples with

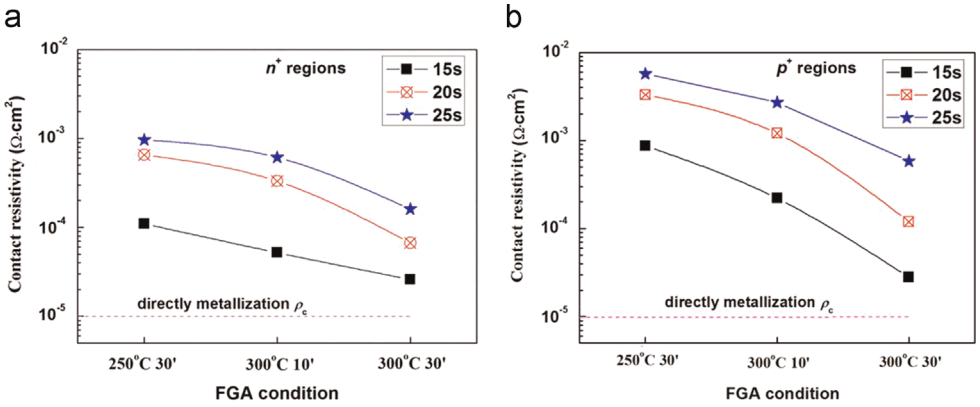

Fig. 3. Contact resistivity dependence on FGA condition for laser doped (a) n^+ and (b) p^+ regions with different oxidation times. The directly metalized ρ_c values are shown as a reference. Lines provide a guide to the eyes.

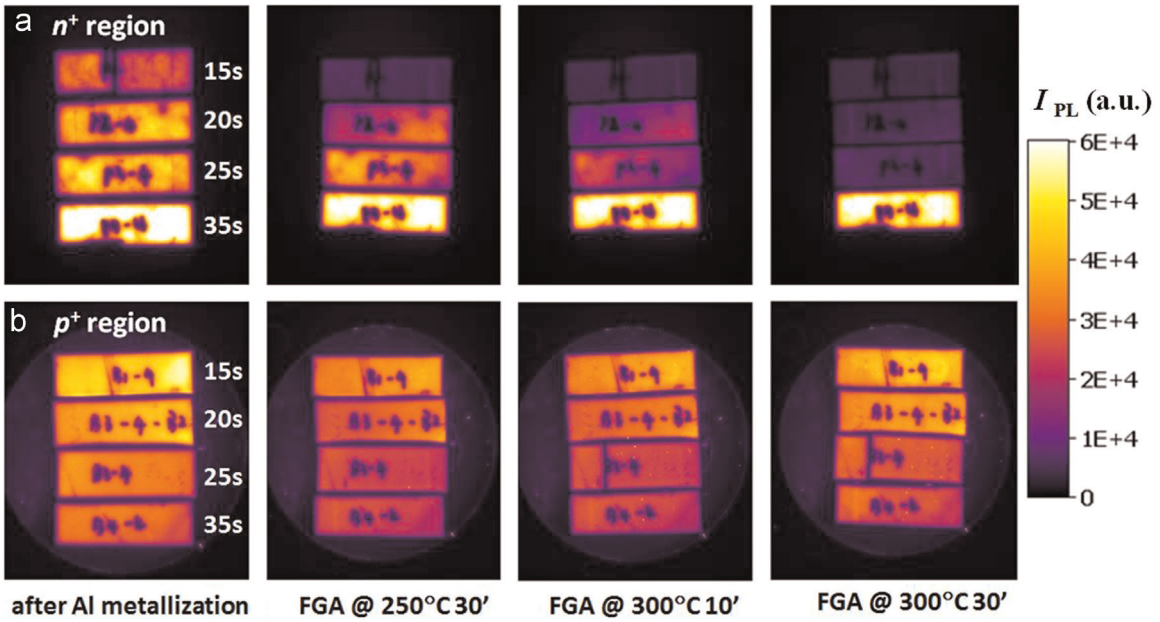

Fig.4. PL images of TLM strips of laser doped (a) n^+ and (b) p^+ regions under different FGA conditions. Four samples with different SiO_2 thicknessess are shown together. The TLM contact pad patterns were defined at the rear side after Al evaporation, and the front side was passivated with the SiO_2/a-Si:H stack. The PL images of n^+ regions were acquired with the same PL parameters, and as were the p^+ regions. PL images of n^+ and p^+ TLM strips were acquired with different PL parameters.

increasing oxide time of 15, 20 and 25 s, respectively. As the FGA temperature and time increase, the I_{PL} of the samples increases instead of decreasing. The results indicate that the passivation quality was improved during the FGA processes. As mentioned above, the p^+ region may mainly rely on the passivation of a-Si:H. An enhanced FGA temperature could cause the interaction between Al and SiO_2, and therefore eliminates the hydrogen diffusion barrier and improve the passivation performance. The increased I_{PL} of the TLM strips with increasing FGA temperatures and times supports this assumption.

3.3. Efficiency potential of an IBC solar cell with laser doped n^+ and p^+ regions

Recently, IBC solar cells with laser doped local n^+ and p^+ regions as well as laser ablation for contact opening have been fabricated at the ANU, and a champion cell efficiency of 19.1% has been achieved with a simplified fabrication process [42]. The efficiency is mainly limited by the high contact resistivity and recombination at the local laser doped regions. The simulation revealed that an efficiency potential of 24% could be achieved with all laser doped IBC cells [43]. The implementation of the proposed passivated contact to laser doped n^+ and p^+ regions into IBC solar cells will not only contribute to the cell efficiency due to a reduced recombination and contact resistivity, but also reduce the fabrication complexity significantly. The complex doping, passivation and contact opening at rear side of IBC solar cells could be achieved by the implementation of the SiO_2/a-Si:H passivated contact to localized laser doped n^+ and p^+ regions developed in this work. All the high temperature diffusion and mask steps, as well as the high cost patterning steps will be eliminated, which will significantly reduce the processing time and cost, degradation in bulk lifetime, and the potential for introducing contaminants. Industrial-feasible, high-efficiency IBC solar cells are expected to fabricate at a low cost by the implementation of the passivated contact to laser doped n^+ and p^+ regions.

Table 2
Parameters used in the Quokka simulations.

Parameters	Value
Cell thickness	160 μm
n^+ FSF sheet resistance	300 Ω/□
n^+ FSF J_{oe}	10 fA/cm^2
n-Type bulk resistivity	2.5 Ω cm
Bulk lifetime	4000 μs
Contact shape	Square
p^+ Emitter contact size	150 × 150 μm^2
n^+ BSF contact size	200 × 200 μm^2
Laser doped p^+ emitter shape	Square
p^+ Emitter half width (x and y)	75 by 75 μm
p^+ Emitter sheet resistance	490 Ω/□
p^+ Emitter J_{oe}-passivated	860 fA/cm^2
p^+ Emitter J_{oe}-contacted	860 fA/cm^2
p^+ Emitter contact resistance	5.7×10^{-3} Ω cm^2
Gap width	50 μm
Gap area J_{oe}-passivated	10 fA/cm^2
Laser doped n^+ BSF shape	Square
n^+ BSF half width (x and y)	100 by 100 μm
n^+ BSF sheet resistance	280 Ω/□
n^+ BSF J_{oe}-passivated	47 fA/cm^2
n^+ BSF J_{oe}-contacted	47 fA/cm^2
n^+ BSF contact resistance	9.6×10^{-4} Ω cm^2
External series resistance	0.2 Ω cm^2
Shut resistance	1×10^5 Ω cm^2

Simulation using Quokka is undertaken to explore the potential efficiency of IBC solar cell with the passivated contact to laser doped n^+ and p^+ regions. The main electrical parameters and inputs needed for the simulations have been obtained from the sample n^+-1 and p^+-1, as summarized in Table 2. We have assumed that the passivation degradation of the laser doped n^+ and p^+ regions after FGA anneals at 250 °C for 30 min could be neglected, and the J_o and the ρ_c values obtained by FGA at 250 °C were used. The J_o values of the contacted area were assumed to be equal to the J_o values in the non-metallized regions based on the PL image results in Fig. 4 as well as the conclusion from previous work [23]. Because of the poor electrical properties of laser doped p^+ regions, we consider an unit cell as sketched in Fig. 5a with smaller laser doped p^+ region (150×150 μm^2) and larger n^+ region (200×200 μm^2) with a square shape. The SiO_2/a-Si:H stack could provide excellent passivation to n-type base resistivity silicon with a J_o of ~10 fA/cm^2, and this value was used for the passivated gap region. By considering the operational possibility of excimer lasers, a rear pitch of 400 μm with gap width of 50 μm was adopted. Other simulated cell parameters include 2.5 Ω cm n-type bulk resistivity, bulk recombination according to the Richter Auger model [44], an industrially feasible water thickness of 160 μm, a typical AM1.5 G uniform generation profile yielding a generation current of 42 mA/cm^2, and a low series resistance of 0.2 Ω cm^2.

Fig. 5b shows the simulated light I–V curve of as-proposed IBC solar cell shown together with the free energy loss analysis (FELA) at the maximum power point (MPP). An efficiency of 23.0% can be achieved on the simplified n-type IBC cell with non-optimized parameters. The simulated FELA at MPP revealed that recombination and resistive losses are the main limit for the cell efficiency. According to the FELA output data, the recombination and resistance at p^+ emitter are identified as the major losses, which could be explained by the relatively high J_o values (860 fA/cm^2) and ρ_c value (5.7×10^{-3} Ω cm^2) at the p^+ region. To further increase the cell efficiency, the main task is to improve the passivation quality and contact resistivity therefore decrease the J_o and ρ_c of laser

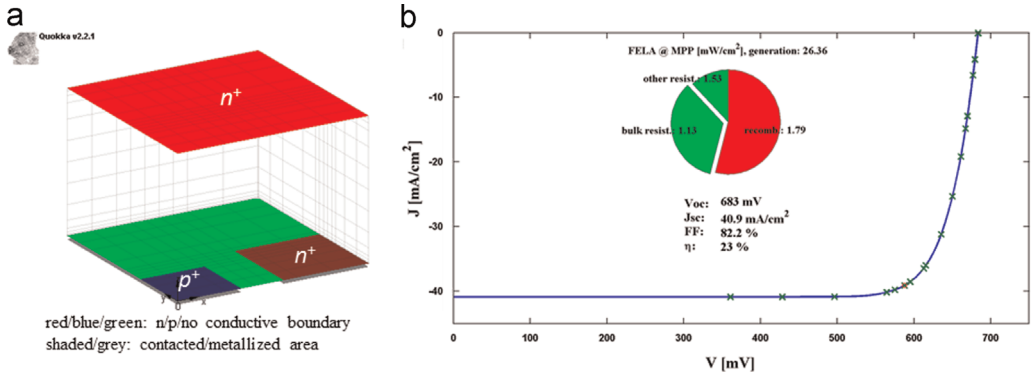

Fig. 5. (a) Unit cell with laser doped local p^+ emitter and n^+ BSF as produced by Quokka and (b) simulated light I–V curve based on the parameters listed in Table 2, shown together with the free energy loss analysis at MPP.

doped p^+ emitter. A fast etch back to remove the high-defected surface region after laser doping or a post high temperature oxidation after laser doping may improve the passivation performance of SiO_2/a-Si:H stack on laser doped p^+ region. Moreover, a longer FGA at 250 °C may further decrease the ρ_c value, as Bullock et al. reported that ρ_c appears to saturate to a value after FGA at 250 °C for 40 min for the diffused regions [23].

4. Conclusions

Passivated contacts to laser doped n^+ and p^+ regions with a tunnel SiO_2/a-Si:H stack have been investigated. The SiO_2/a-Si:H stack provides excellent passivation to laser doped n^+ regions, whereas a lower passivation performance is observed on laser doped p^+ regions. A post FGA at 400 °C could improve the passivation to laser doped p^+ regions to some extent. With the optimal tunnel SiO_2 thickness and proper FGA condition, appreciable contact resistivity values have been achieved on both laser doped n^+ and p^+ regions while maintaining acceptable surface passivation. The alloying between a-Si:H and aluminum during the FGA is considered as the crucial mechanism in forming the contact. The implementation of the passivated contact to laser doped n^+ and p^+ regions could significantly contribute to the IBC solar cell efficiency as well as fabrication complexity. Simulated *I–V* curve of the n-type IBC solar cell shows an efficiency of up to 23.0% with the non-optimized experimental parameters. A further improvement could be expected by improving the passivation performance to laser doped p^+ regions as well as the cell structure design.

Acknowledgment

The authors acknowledge financial support from the Australian Renewable Energy Agency (ARENA) (No. 6-F007) under the Postdoctoral Fellowship. We also would like to thank Andres Cuevas (ANU) for the helpful discussion and S. Phang (ANU) for helping with PECVD a-Si:H deposition.

References

[1] J. Zhao, A. Wang, Martin A. Green, 24.5% efficiency silicon PERT cells on MCZ substrates and 24.7% efficiency PERL cells on FZ substrates, Prog. Photovolt. 7 (1999) 471–474.
[2] E. Kerschaver, G. Beaucarne, Back-contact solar cells: a review, Prog. Photovolt. 14 (2006) 107–123.
[3] M. Kim, D. Kim, D. Kim, Y. Kang, Influence of laser damage on the performance of selective emitter solar cell fabricated using laser doping process, Sol. Energy Mater. Sol. Cells 132 (2015) 215–220.
[4] D. Lin, M. Abbott, P.H. Lu, B. Xiao, B. Hallam, B. Tjahjono, S. Wenham, Incorporation of deep laser doping to form the rear localized back surface field in high efficiency solar cells, Sol. Energy Mater. Sol. Cells 130 (2014) 83–90.
[5] B. Steinhauser, U. Jäger, J. Benick, M. Hermle, PassDop rear side passivation based on Al_2O_3/a-SiC_x: B stacks for p-type PERL solar cells, Sol. Energy Mater. Sol. Cells 131 (2014) 129–133.
[6] G. Xu, B. Hallam, Z. Hameiri, C. Chan, Y. Yao, C. Chong, S. Wenham, Over 700 mV implied V_{oc} on p-type CZ silicon solar cells with double-sided laser doping, Energy Procedia 33 (2013) 33–40.
[7] I. Martín, P. Ortega, M. Colina, A. Orpella, G. López, R. Alcubilla, Laser processing of Al_2O_3/a-SiC_x:H stacks: a feasible solution for the rear surface of high-efficiency p-type c-Si solar cells, Prog. Photovolt. 21 (2013) 1171–1175.
[8] T.C. Roder, S.J. Eisele, P. Grabitz, C. Wagner, G. Kulushich, J.R. Kohler, J.H. Werner, Add-on laser tailored selective emitter solar cells, Prog. Photovolt. 18 (2010) 505–510.
[9] Z. Hameiri, L. Mai, A. Sproul, S.R. Wenham, 18.7% Efficient laser-doped solar cell on p-type Czochralski silicon, Appl. Phys. Lett. 97 (2010) 222111.
[10] E. Schneiderlöchner, R. Preu, R. Lüdemann, S.W. Glunz, Laser-fired rear contacts for crystalline silicon solar cells, Prog. Photovolt. 10 (2002) 29–34.
[11] M. Dahlinger, B. Bazer-Bachi, T.C. Röder, J.R. Köhler, R. Zapf-Gottwick, J.H. Werner, 22.0% Efficient laser doped back contact solar cells, Energy Procedia 38 (2013) 250–253.
[12] M. Ametowobla, G. Bilger, J.R. Kohler, J.H. Werner, Laser induced lifetime degradation in p-type crystalline silicon, J. Appl. Phys. 111 (2012) 114515.
[13] Z. Hameiri, L. Mai, T. Puzzer, S.R. Wenham, Influence of laser power on the properties of laser doped solar cells, Sol. Energy Mater. Sol. Cells 95 (2011) 1085–1094.
[14] A. Fell, D. Walter, X. Yang, S. Surve, E. Franklin, K. Weber, D. MacDonald, Quantitative surface recombination imaging of single side processed silicon wafers obtained by photoluminescence modelling, Energy Procedia 55 (2014) 63–70.
[15] M.A. Green, A.W. Blakers, N.R. Willison, T. Szpitalak, E.M. Keller, E. Gauja, P.J. Bart, The MINP solar cell – a new high voltage, high efficiency silicon solar cell, in: Proceedings of the 15th IEEE Photovoltaics Specialist Conference, 1981, pp. 1405–1408.
[16] K. Jäger-Hezel, W. Schmidt, W. Heit, K.D. Rasch, Improved large area MIS-contacted silicon solar cells, in: Proceedings of the 13th European Photovoltaic Solar Energy Conference, 1995, pp. 1515–1518.
[17] A. Metz, R. Hezel, Recorded efficiency above 21% for MIS-contacted diffused junction silicon solar cells, in: Proceedings of the 26th IEEE Photovoltaics Specialist Conference, 1997, pp. 283–286.
[18] X. Loozen, J.B. Larsen, F. Dross, M. Aleman, T. Bearda, B.J. O'Sullivan, I. Gordona, J. Poortmans, Passivation of a metal contact with a tunneling layer, Energy Procedia 21 (2012) 75–83.
[19] D. Garcia-Alonso, S. Smit, S. Bordihn, W. Kessels, Silicon passivation and tunneling contact formation by atomic layer deposited Al_2O_3/ZnO stacks, Semicond. Sci. Technol. 28 (2013) 082002.
[20] J. Bullock, D. Yan, A. Cuevas, Passivation of aluminium-n^+ silicon contacts for solar cells by ultrathin Al_2O_3 and SiO_2 dielectric layers, Phys. Status Solidi RRL 7 (2013) 946–949.
[21] J. Bullock, D. Yan, Y. Wan, A. Cuevas, B. Demaurex, A. Hessler-Wyser, S. De Wolf, Amorphous silicon passivated contacts for diffused junction silicon solar cells, J. Appl. Phys. 115 (2014) 163703.
[22] J. Bullock, A. Cuevas, D. Yan, B. Demaurex, A. Hessler-Wyser, S. De Wolf, Passivated contacts to n^+ and p^+ silicon based on amorphous silicon and thin dielectrics, in: Proceedings of the 40th IEEE Photovoltaic Specialist Conference, Denver, USA, 2014, pp. 3442–3447.
[23] J. Bullock, D. Yan, A. Cuevas, B. Demaurex, A. Hessler-Wyser, S. De Wolf, Amorphous silicon enhanced metal–insulator–semiconductor contacts for silicon solar cells, J. Appl. Phys. 116 (2014) 163706.
[24] B.-Y. Tsaur, G.W. Turner, J.C.C. Fan, Efficient Si solar cells by low-temperature solid-phase epitaxy, Appl. Phys. Lett. 39 (1981) 749.
[25] M.S. Hapue, H.A. Naseem, W.D. Brown, Aluminium-induced crystallization and counter-doping of phosphorous-doped hydrogenated amorphous silicon at low temperatures, J. Appl. Phys. 79 (1996) 7529.
[26] H. Plagwitz, M. Nerdling, N. Ott, H.P. Strunk, R. Brendal, Low-temperature formation of local Al contacts to a-Si:H passivated Si wafers, Prog. Photovolt.: Res. Appl. 12 (2004) 47.
[27] J. Bullock, A. Cuevas, C. Samundsett, D. Yan, J. McKeon, Y. Wan, Simple silicon solar cells featuring an a-Si:H enhanced rear MIS contact, Sol. Energy Mater. Sol. Cells 138 (2015) 22–25. http://dx.doi.org/10.1016/j.solmat.2015.02.030.
[28] X. Yang, J. Bullock, Q. Bi, K. Weber, High efficiency n-type silicon solar cells featuring passivated contact to laser doped regions, Appl. Phys. Lett. 106 (2015) 113901.
[29] R.A. Sinton, A. Cuevas, Contactless determination of current–voltage characteristics and minority-carrier lifetimes in semiconductors from quasi-steady-state photoconductance data, Appl. Phys. Lett. 69 (1996) 2510.
[30] G.K. Reeves, H.B. Harrison, Obtaining the specific contact resistance from transmission-line model measurements, IEEE Electron Device Lett. 3 (1982) 111–113.
[31] T. Trupke, R.A. Bardos, M.C. Schubert, W. Warta, Photoluminescence imaging of silicon wafers, Appl. Phys. Lett. 89 (2006) 044107.
[32] E. Peiner, A. Schlachetzki, D. Krüger, Doping profile analysis in Si by electrochemical capacitance-voltage measurements, J. Electrochem. Soc. 142 (1995) 576–580.
[33] D.E. Kane and R.M. Swanson, Measurement of the emitter saturation current by a contactless photoconductivity decay method, in: Proceedings of the 18th IEEE Photovoltaic Specialist Conference, Las Vegas, USA, 1985, pp. 578–583.
[34] A. Fell, K.C. Fong, K.R. McIntosh, E. Franklin, A.W. Blakers, 3-D simulation of interdigitated-back-contact silicon solar cells with Quokka including perimeter losses, IEEE J. Photovolt. 4 (2014) 1040–1045.
[35] B. Hoex, J. Schmidt, R. Bock, P.P. Altermatt, M. Sanden, W.M.M. Kessels, Excellent passivation of highly doped p-type Si surfaces by the negative-charge-dielectric Al_2O_3, Appl. Phys. Lett. 91 (2007) 112107.
[36] M.J. Kerr, J. Schmidt, A. Cuevas, J.H. Bultman, Surface recombination velocity of phosphorus-diffused silicon solar cell emitters passivated with plasma enhanced chemical vapor deposited silicon nitride and thermal silicon oxide, J. Appl. Phys. 89 (2011) 3821–3826.
[37] I.R.C. Post, P. Ashbum, G.R. Wolstenholme, Polysilicon emitters for bipolar transistors: a review and re-evaluation of theory and experiment, IEEE Trans. Electron Devices 39 (1992) 1717–1739.
[38] G.R. Wolstenholme, N. Jorgensen, P. Ashburn, G.R. Booker, An investigation of the thermal stability of the interfacial oxide in polycrystalline silicon emitter bipolar transistors by comparing device results with high-resolution electron microscopy observations, J. Appl. Phys. 61 (1987) 225.
[39] J.Y. Gan, R.M. Swanson, Polysilicon emitters for silicon concentrator solar cells, in: Proceedings of the 21st IEEE Photovoltaic Specialist Conference, USA, 1990, pp. 245–250.

[40] R. Peibst, U. Romer, K.R. Hofmann, B. Lim, T.F. Wietler, J. Krugener, N. Harder, R. Brendel, A simple model describing the symmetric *I–V* characteristics of p polycrystalline Si/n monocrystalline Si, and n polycrystalline Si/p monocrystalline Si junctions, IEEE J. Photovolt. 4 (2014) 841.
[41] X. Yang, D. Macdonald, A. Fell, A. Shalav, Lujia Xu, D. Walter, T. Ratcliff, E. Franklin, K. Weber, R. Elliman, Imaging of the relative saturation current density and sheet resistance of laser doped regions via photoluminescence, J. Appl. Phys. 114 (2013) 053107.
[42] E. Franklin, K.C. Fong, K.R. McIntosh, A. Blakers, K. Teng, D. Wang, S. Ngwe, M. Stocks, E. Wang, N. Grant, A. Fell, Y. Wan, Y. Yang, X. Zhang, Z. Feng, P.J. Verlinden, Design, fabrication and characterisation of a 24.4% efficient interdigitated back contact solar cell, Prog. Photovolt. (2014), http://dx.doi.org/10.1002/pip.2556.
[43] A. Fell, A. Surve, E. Franklin, K. Weber, Characterisation of laser-doped localised p-n Junctions for high efficiency silicon solar cells, IEEE Trans. Electron Devices 61 (2014) 1943–1949.
[44] A. Richter, S.W. Glunz, F. Werner, J. Schmidt, A. Cuevas, Improved quantitative description of auger recombination in crystalline silicon, Phys. Rev. B 86 (2012) 165202.